Automated Inspection Methodology of Wall Rebar Spacing and Diameters Using Laser Scanning

Philgu Kim[1], Jungyeon Kim[1], Jeongwoon Choi[1], Seokho Chi[1]

[1]Department of Civil and Environmental Engineering, Seoul National University, Republic of Korea
leophilgu@snu.ac.kr, janykjy@snu.ac.kr, cjw5428@snu.ac.kr, shchi@snu.ac.kr

Abstract

This study presents a methodology for the automated inspection of rebar diameters and spacing in wall structures using a laser scanner. Previous studies conducted the methods in controlled laboratory environments, and primarily focused on predicting rebar diameters larger than 10 mm. However, these methods have difficulties applying to real-world construction sites which have rebars on bent, and limited scanning positions. This research was performed on an actual construction site where small-diameter rebars (10 mm) were arranged in double layers. To address the curvature presented in rebar arrangement surfaces, a new methodology was introduced; linearity was analyzed to detect the complex rebar arrangements. The spacing of the rebars was calculated by projecting the point clouds onto an axis aligned with the rebar arrangement. Rebar diameters were estimated through RANdom Sample Consensus (RANSAC) circle fitting. The results demonstrate that the proposed methodology successfully modeled distorted rebar structures presented in construction sites, enabling accurate extraction and prediction of rebar objects. This approach can replace labor-intensive manual inspections, ensuring accurate and reliable verification against design specifications.

Keywords

Laser scanner; Point cloud; Automated inspection, Rebar spacing, Rebar diameter

1 Introduction

To ensure structural safety in reinforced concrete construction, rebars must be placed precisely at the designated locations and with the appropriate sizes specified in the design drawings. The placement and size of rebars directly play a critical role in determining the load-bearing capacity of reinforced concrete [6]. Improperly arranged rebars during concrete casting can result in structural failures. Therefore, rigorous inspections of rebar placement are essential.

Traditionally, rebar placement inspections in construction sites are performed visually by inspectors who physically traverse the site, using tape measures to check spacings and sizes. As the work area expands, these inspections become increasingly time-consuming, labor-intensive, and hazardous, as inspectors must move across all rebar-equipped areas [1].

To overcome the challenges of manual inspections, numerous studies have aimed to automate the rebar inspection process. Among these approaches, laser scanners have gained significant attention for their ability to capture point cloud data of rebar arrangements and to subsequently compute rebar diameters and spacing [2]. However, previous studies have conducted experiments under laboratory conditions. These studies primarily focused on predicting rebar diameters and spacing under optimal scanning angles, with most cases involving rebar diameters larger than 10 mm. In contrast, actual construction sites feature highly complex rebar arrangements. Thus, scanning positions are often limited and conditions, which differ significantly from laboratory settings, make it challenging to accurately detect rebars on bent or irregular surfaces. Consequently, these methods are unable to recognize rebars in diverse positions or with small diameters. To address these limitations, this study focused on scanning rebars arranged at real construction sites, segmenting each rebar, and automatically predicting their diameters and spacing. Furthermore, the proposed method can be utilized in Scan-to-BIM (Building Information Modeling) workflows by enabling the automated generation of 3D as-built rebar models. This approach ultimately contributes to improving construction quality control, structural verification, and digital lifecycle management in reinforced concrete construction.

2 Literature Review

Point clouds are widely used owing to their high efficiency and accuracy [10, 11, 12, 13, 14, 15]. Previous studies have created and analyzed point clouds generated by Terrestrial Laser Scanners (TLS) to automate rebar inspection [2, 3, 4, 5, 6]. These studies typically focused on separating vertical and horizontal rebars to estimate both the diameter of each segment and the spacing between segments. For instance, Kim et al. [2] employed RANSAC [9] to segment individual rebars and applied Density-based Modeling (DBM) to enhance the classification accuracy for rebar diameter estimation. Li et al. [17] presented a scan planning method to select the optimal scan position of laser scanner for improving the rebar inspection accuracy. However, these methods are conducted under laboratory conditions. Most of previous studies focused on predicting rebar diameters and spacing based on optimal scanning angles, primarily focusing on rebars larger than 10 mm in diameter. In real-world scenarios, rebar arrangements are far complex, and scanning positions are frequently constrained. Likewise, the environmental differences from laboratory settings pose significant challenges in accurately detecting rebars on curved of uneven surfaces.

To address these gaps, this study proposes methodology for two purposes: (1) rebar detection using laser scans in complex construction sites, and (2) diameter and spacing prediction for small-diameter rebars.

3 Methodology

3.1 Research Framework

Figure 1 illustrates the framework of this study: rebar scanning and 3D reconstruction, data preprocessing, rebar detection, and diameter and spacing prediction. During the rebar detection stage, planarity, linearity, and iterative RANSAC are utilized to remove formwork and base surfaces. Subsequently, double-layered rebar arrangements are distinguished through Otsu thresholding. For spacing prediction, projection algorithm and cubic spline interpolation are used to predict the location of vertical rebars. For diameter prediction, rebars are divided into individual instances and projected onto the surface perpendicular to the first axis of Principal Component Analysis (PCA). The diameters are then predicted using circle fitting based on the RANSAC method.

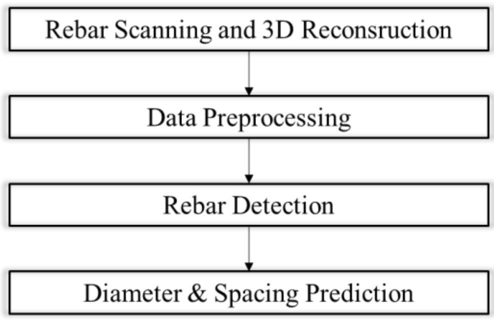

Figure 1 Research framework

3.2 Rebar Scanning and 3D Reconstruction

At an actual construction site, a wall rebar structure with 10 mm diameter rebars arranged in double layers at 300 mm intervals beside the formwork was scanned. The scanning was performed from five different positions using a FARO Focus M laser scanner. The point clouds collected from each position were subsequently combined into one unified point cloud using FARO Scene software, as shown in Figure 2.

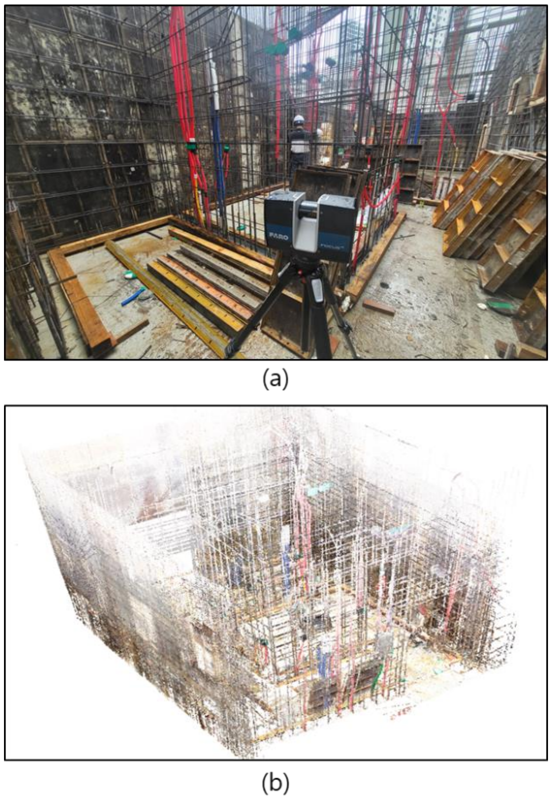

Figure 2 (a) Scanning of wall rebar arrangement; (b) 3D point cloud reconstruction of wall rebar arrangement

3.3 Data Preprocessing

Prior to analyzing the rebars, noise was removed using the Statistical Outlier Removal (SOR) method [16]. In this process, points whose average distance to their 10 nearest neighbors exceeds twice the standard deviation threshold were considered outliers and removed.

3.4 Rebar Detection

The preprocessed point cloud contains various elements, including rebars, formwork surfaces, materials, and floor surfaces. To extract the rebar point cloud, unnecessary information must be removed. As shown in Figure 2(b), rebars exhibit an elongated linear shape in the point cloud, whereas other elements do not. To distinguish these, the linearity and planarity of the neighboring point cloud data were analyzed. For this analysis, the Radius Nearest-Neighbor Covariance (RNCC) method was applied [8]. RNCC computes the eigenvalues of the covariance matrix for points within a given radius *r*, representing the degree of data dispersion (see Equation (1)).

$$Cov = \frac{1}{N}\sum_{i=1}^{N}(p_i - \bar{p})(p_i - \bar{p})^T \qquad (1)$$

In this content, N denotes the number of neighboring points within radius r, p_i is the coordinate vector of each neighboring point, and $\bar{p}$ is the centroid of the neighboring points. The first eigenvalue λ_1 represents the variance in the direction where the data is most dispersed. The second and third eigenvalues, λ_2 and λ_3, correspond to the variances in the second and third most dispersed directions, respectively.

By calculating the eigenvalues of the covariance matrix, the linearity (see Equation (2)) and planarity (see Equation (3)) of the point cloud can be evaluated. For linear data, λ_1 is large and λ_2 is small; therefore, a larger $\lambda_1 - \lambda_2$ value indicates greater linearity. For planar data, both $\lambda_1, and\ \lambda_2$ are large while $\lambda_3$is very small; thus, a larger $\lambda_2 - \lambda_3$ value indicates higher planarity.

$$L_\lambda = \frac{\lambda_1 - \lambda_2}{\lambda_1 + \lambda_2 + \lambda_3} \qquad (2)$$

$$P_\lambda = \frac{\lambda_2 - \lambda_3}{\lambda_1 + \lambda_2 + \lambda_3} \qquad (3)$$

Using the obtained linearity and planarity data, formwork surfaces with high planarity can be removed, while rebar point cloud data with high linearity can be segmented.

Figure 3 visually represents the distribution of linearity and planarity. As shown in Figure 3(c), the formwork appears in blue, indicating low linearity, while the rebars appear in red, indicating high linearity. In contrast, Figure 3(d) shows that the formwork has high planarity, whereas the rebars exhibit low planarity. By setting thresholds based on the distribution of linearity and planarity, filtering was applied to extract the rebar point cloud.

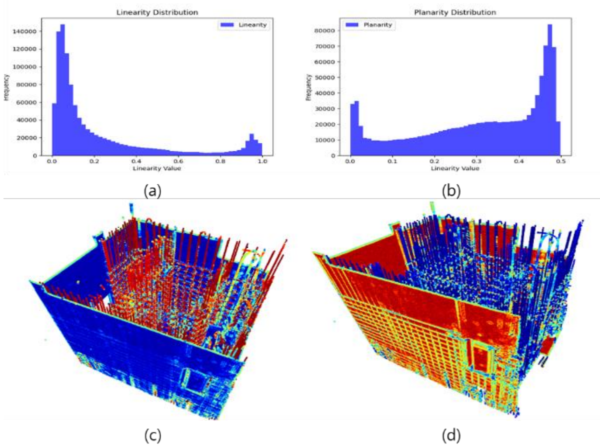

Figure 3 (a) Linearity distribution of point cloud; (b) Planarity distribution of point cloud; (c) Linearity expression of point cloud (red: high linearity, blue: low linearity); (d) Planarity expression of point cloud (red: high planarity, blue: low planarity)

A filtering threshold of 0.3 was applied to the linearity distribution, resulting in a point cloud that excludes the formwork and the floor surface, as shown in Figure 4. However, unnecessary noise still remained, such as construction materials.

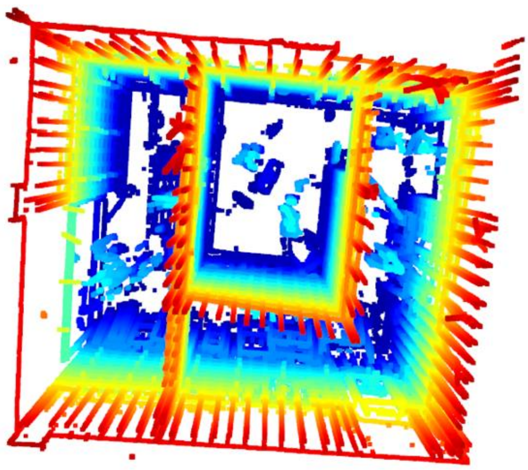

Figure 4 Filtered point cloud by linearity threshold

Such remaining noise in the point cloud needs to be removed, and the rebars arranged at various angles must be separated to calculate their spacing. To achieve this, the RANSAC method was employed. RANSAC fits a specific model to the input data and identifies inliers that best conform to the model. Since rebar-arranged surfaces typically have a planar shape, fitting a plane model in a 3D space using RANSAC enables the extraction of the rebar-arranged surface, which is identified as inliers. By removing the extracted points and reapplying RANSAC to the remaining data, other rebar surfaces can be identified. This iterative process continues until no surface contains more than a predefined number of inliers, at which point RANSAC terminates. This method allows for the identification of all rebar surfaces while simultaneously removing noise, as illustrated in Figure 5.

Figure 5 Iterative RANSAC of filtered point cloud

The rebar surface segments obtained through iterative RANSAC consist of rebars arranged in double layers. To further distinguish the two rebar surfaces, a plane is recalculated using RANSAC, and the point distribution by distance is analyzed, revealing two distinct peaks at different locations, as shown in Figure 6(a). To divide the data into two groups, Otsu Thresholding was applied. This method determines an optimal threshold by maximizing the between-class variance in a histogram, allowing for the separation of the double-layered rebar data (Figure 6(b)). The results are visualized in Figure 7.

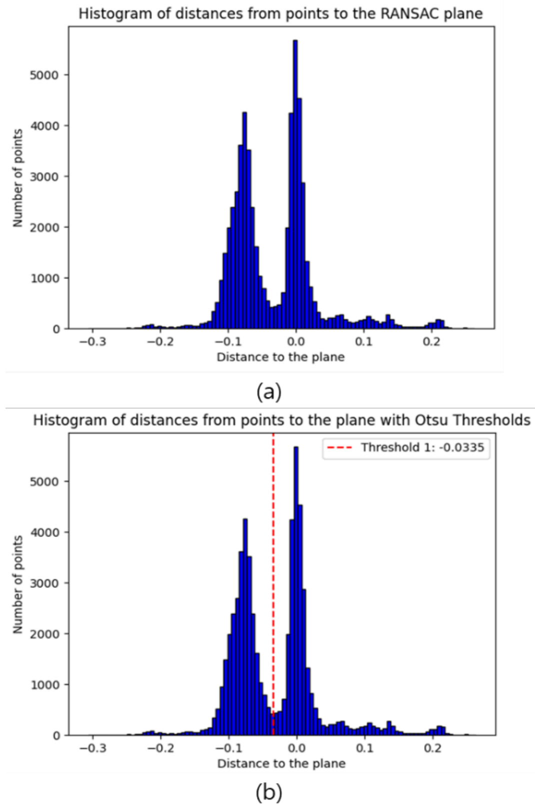

Figure 6 (a) Histogram of distances from points to the RANSAC plane; (b) Histogram of distances from points to the plane with Otsu Thresholds

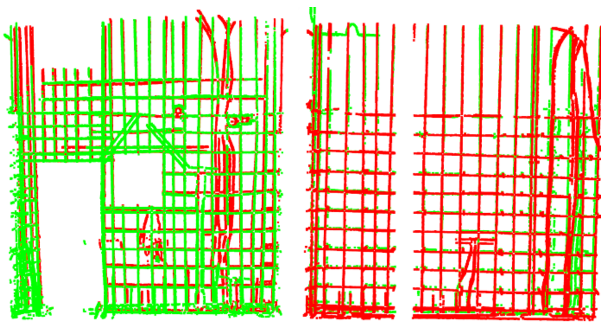

Figure 7 Visualization of double-layered rebar separation results

The study aimed to predict the rebar arrangement (i.e., spacing and diameter) of the actual double-layered rebar surfaces measured. Therefore, one-layered rebar surfaces separated in Figure 7 was used for further research.

3.5 Diameter & Spacing Prediction

Using the rebar point cloud obtained through the previous process, the rebar diameter and spacing could be estimated. In previous studies, rebar surfaces were assumed to be perfectly planar, a feasible assumption in controlled laboratory environments. Under these conditions, RANSAC was used to separate horizontal and vertical rebars. However, as shown in Figure 8, the distance between the rebar point cloud and the RANSAC plane is visualized using color variations, with red indicating greater distances and blue representing shorter distances. This exhibits that the actual rebar surfaces in the field poses curvature rather than a perfect planar shape. This presents a limitation: in the presence of curvature, RANSAC can fit incorrect planes, leading to the spurious-plane problem [7]. This issue occurs in 3D point cloud segmentation, where the algorithm incorrectly detects planes that do not actually exist in the data. This limitation makes it difficult to apply the rebar segmentation methods proposed in previous studies to real-world construction sites. Accordingly, this study proposes a novel method for predicting the spacing of rebars that can be applied even when the rebars are bent in actual construction sites. Based on the rebar spacing data, we further suggest a methodology for estimating the rebar diameter.

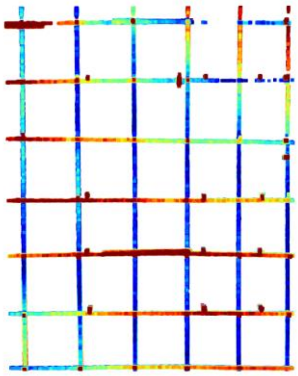

Figure 8 Visualization of distance from RANSAC plane (red: greater distance, blue: shorter distance)

3.5.1 Rebar Spacing Prediction

To estimate the spacing between rebars, the 3D points were projected onto a 1D axis aligned parallel to the rebar arrangement direction. Figure 9 shows histograms of the point distributions when the points are projected onto the horizontal and vertical axes. These histograms were normalized into curves using cubic spline interpolation, and the local maxima exceeding a specific threshold were identified, as shown in Figure 10. The locations of these local maxima on the normalized point density curve correspond to the centers of rebars aligned perpendicular to the projection axis. The spacing between horizontal and vertical rebars can thus be determined by calculating the distances between adjacent local maxima.

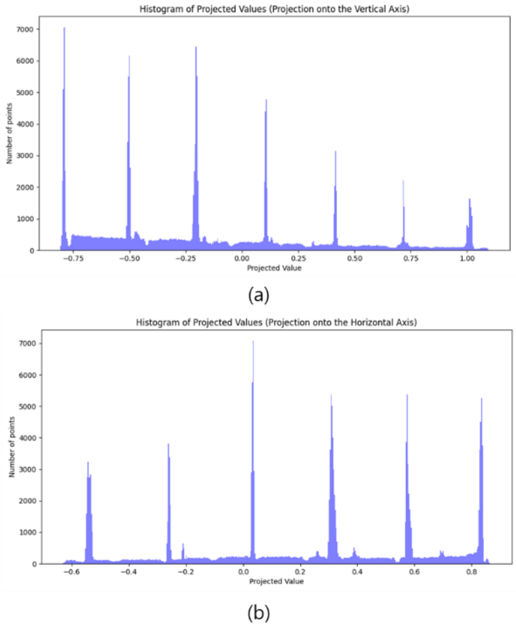

Figure 9 (a) Histogram of projected values (projection onto the vertical axis); (b) Histogram of projected values (projection onto the horizontal axis)

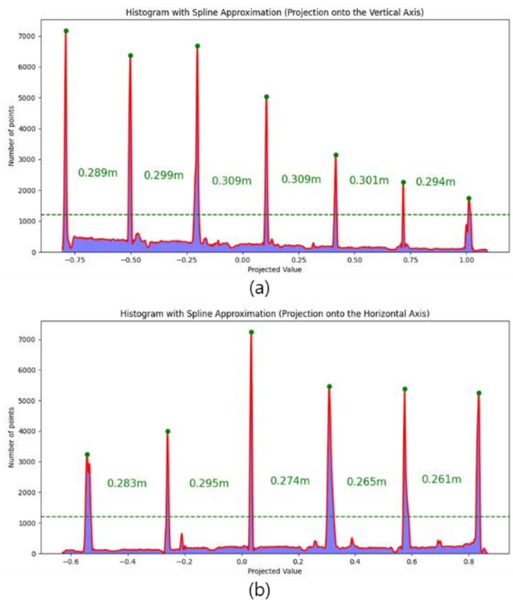

Figure 10 (a) Histogram with spline approximation and horizontal spacing prediction (projection onto the vertical axis); (b) Histogram with spline approximation and vertical spacing prediction (projection onto the horizontal axis)

The comparison between the predicted rebar spacing and the manually measured spacing is shown in Table 1.

Table 1 The comparison between the predicted rebar spacing and the manually measured spacing (mm)

		Spacing No.						Average error (mm)	Average accuracy (%)
		1	2	3	4	5	6		
Horizontal rebar spacing	Predicted	289	299	309	309	301	294		
	Measured	291	305	308	317	295	282		
	Error	2	6	1	8	6	12	6	98
Vertical rebar spacing	Predicted	283	295	274	265	261			
	Measured	284	287	282	268	252			
	Error	1	8	8	3	9		6	98

The measured spacing values refer to the manually measured spacing using a measuring tape. As shown in Table 1, the average spacing error for both horizontal and vertical rebars was 6 mm, which indicates an average error rate of 2%. This demonstrates that the proposed automated rebar spacing prediction method achieved an average accuracy of 98%.

3.5.2 Rebar Diameter Prediction

To estimate the diameter of the rebars, the cross-sectional data of each rebar was extracted. As shown in Figure 11, the segments between rebars were cropped based on the previously obtained rebar spacing information. These segments were then divided using Density-Based Spatial Clustering of Applications with Noise (DBSCAN). For each cluster, PCA was applied to calculate the first principal axis, which corresponds to the direction with the largest variance. The points were then projected onto a plane perpendicular to this principal axis. Since scanned rebars will show a circular shape in the projected points, a circle fitting algorithm could be used for diameter prediction.

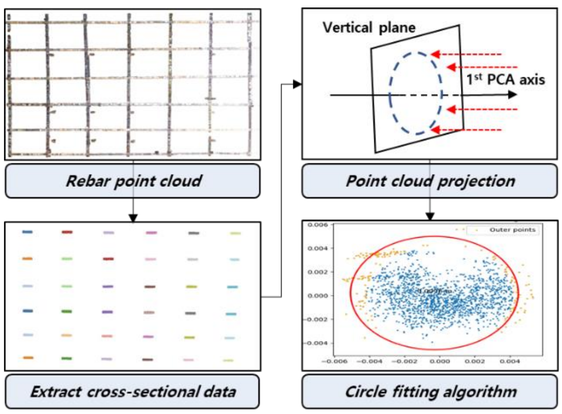

Figure 10 Processing steps for rebar diameter prediction

As the deformed rebars used at the construction site have ribs and lugs, the projected point clouds were generally distributed in circular or semi-circular shapes. However, in order to accurately estimate the diameter of each rebar segment, it is essential to use the outermost distributed points. This is because each segment contains almost no external noise, and the outermost points are likely to represent the outer surface of the rebar. Therefore, circle fitting based on outer points was applied to estimate the rebar diameters. Specifically, for each segment, a center point was determined, and RANSAC-based circle fitting was performed using the top 10% of points with the largest distances from the center. The result example is presented in Figure 12.

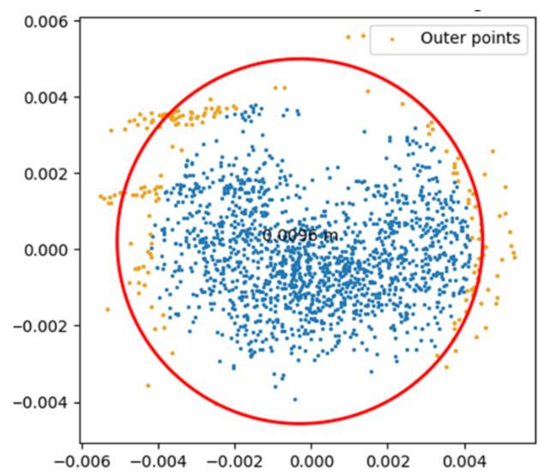

Figure 11 Segment diameter prediction example by extraction of outermost points and RANSAC circle fitting

The predicted rebar diameters were categorized into designations based on their nominal diameters, as shown in Table 2. Each segment was classified by matching its estimated diameter to the closest nominal diameter. These nominal diameters were used as the categories. The predicted diameters for each segment were classified into the nearest nominal diameter among these categories.

Table 2 Type of designation

Designation	Nominal diameter (mm)
D4	4.23
D5	5.29
D6	6.35
D8	7.94
D10	9.53
D13	12.7
D16	15.9
D19	19.1

Since each rebar was divided into multiple segments, the diameter of the rebar was determined by identifying the mode (i.e., most frequent value) of the class within the segment group. This approach helps mitigate prediction deviations caused by local noise in individual segments. It also provides a more effective basis for assessing the classification accuracy of each rebar into its correct nominal diameter, which is important for subsequent use in Scan-to-BIM applications. As shown in Figure 13, the predicted rebar diameters were 6 mm, 8 mm, 10 mm, or 13mm. At the segment level, the accuracy was 72.2%, while at the rebar level, the accuracy was 100%. In comparison, a previous study reported a segment level accuracy of 35.1% and a rebar level accuracy of 56% in estimating the 10 mm rebar diameters [2]. Therefore, the proposed method achieved significantly improved performance.

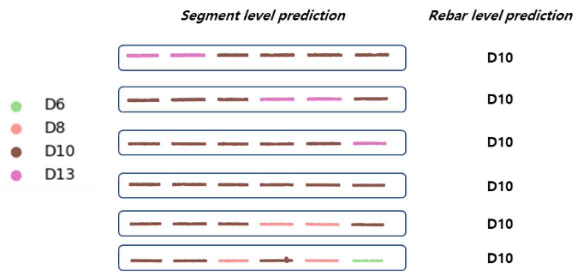

Figure 12 Rebar diameter prediction

4 Conclusion

4.1 Summary & Contribution

This study proposed a methodology for automating rebar arrangement inspection at construction sites. Unlike laboratory conditions, the research was conducted on an actual construction site where small-diameter rebars (10 mm) were arranged in double layers within a wall structure. First, a method for recognizing rebars in complex construction sites was proposed. The rebar was separated from non-rebar structural elements in the point cloud by utilizing the planar and linear characteristics of the objects. Subsequently, the rebar surfaces arranged in various directions were individually segmented using the RANSAC algorithm. A novel approach was introduced to estimate rebar diameters and spacing, even when the rebar surfaces were not perfectly planar. The accuracy of the proposed automated rebar spacing prediction was 98%, and the accuracy of rebar diameter prediction was 72.2% at the segment level and 100% at the rebar level.

Compared to thicker rebars, thinner rebars are more prone to bending or deformation. When the reinforcement surface is distorted, existing methods proposed in previous studies may no longer be applicable. Therefore, the proposed method can be particularly effective for detecting and analyzing small diameter rebars. Also, the proposed methodology can automate the complex and labor-intensive task of inspecting densely arranged rebars using laser scanners on real-world construction sites. Additionally, comparison and analysis with design specifications can ensure safe and accurate rebar arrangement inspection.

The proposed methodology can be further integrated with Scan-to-BIM technologies to support the automated generation of 3D models from scanned point cloud data. Through this process, rebar arrangement results can be accurately reflected in the digital model, enabling the classification of rebar types and the recognition of individual rebar elements within the 3D environment. Such integration allows for more precise modeling of the construction status and facilitates the identification of various components on-site.

4.2 Limitations

Since there were no rebars smaller than 10 mm in the scanned site, the current study was limited to 10 mm-diameter rebars. Further research will be conducted on sites with rebars of smaller or larger diameters.

When extracting rebar information from the point cloud using its linear or planar characteristics, information loss can occur in overlapping regions of rebars. This is due to the reduced linearity caused by distribution of adjacent points in both vertical and horizontal directions. Thus, further work will focus on constructing datasets that include rebar intersection points to enhance the applicability of the proposed method. Additionally, the method for calculating rebar spacing assumes that rebars are arranged vertically; thus, the proposed approach has limitations when rebars are placed diagonally.

Diameter and spacing estimation were performed only for a subset of the separated rebar segments, rather than for the entire dataset. This is because the current method could not effectively handle noise-included data, where other materials were not fully removed from the segmentation process. Future research will focus on addressing this issue.

5 Acknowledgement

This work was supported by the National Research Foundation of Korea(NRF) grant funded by the Korea government(MSIT) (No. RS-2023-00241758).

References

[1] G. A. Washer and C. A. Chang. Guideline for implementing quality control and quality assurance for bridge inspection, *National Cooperative Highway Research Program*, Project 20-07, Task, 252, 2009.

[2] M.-K. Kim, J. P. P. Thedja, H. L. Chi, and D. E. Lee. Automated rebar diameter classification using point cloud data based machine learning. *Automation in Construction*, 122:103476, 2021.

[3] M.-K. Kim, J. P. P. Thedja, and Q. Wang. Automated dimensional quality assessment for formwork and rebar of reinforced concrete components using 3D point cloud data. *Automation in Construction*, 112:103077, 2020.

[4] H. L. Chi, M. K. Kim, K. Z. Liu, J. P. P. Thedja, J. Seo, and D. E. Lee. Rebar inspection integrating augmented reality and laser scanning. *Automation in Construction*, 136:104183, 2022.

[5] X. Yuan, A. Smith, R. Sarlo, C. D. Lippitt, and F. Moreu. Automatic evaluation of rebar spacing using LIDAR data. *Automation in Construction*, 131:103890, 2020.

[6] X. Yuan, A. Smith, F. Moreu, R. Sarlo, C. D. Lippitt, M. Hojati, S. Alampalli, and S. Zhang. Automatic evaluation of rebar spacing and quality using LiDAR data: Field application for bridge structural assessment. *Automation in Construction*, 146:104708, 2023.

[7] L. Li, F. Yang, H. Zhu, D. Li, Y. Li, and L. Tang. An Improved RANSAC for 3D Point Cloud Plane Segmentation Based on Normal Distribution Transformation Cells. *Remote Sens*, 9(5):433, 2017.

[8] W. Zhao, Y. Jiang, Y. Liu, and J. Shu. Automated recognition and measurement based on three-dimensional point clouds to connect precast concrete components. *Automation in Construction*, 133:104000, 2022.

[9] M. A. Fischler and R. C. Bolles. Random sample consensus: a paradigm for model fitting with applications to image analysis and automated cartography, *Commun*, ACM 24 (6):381-395, 1981.

[10] M.-K. Kim, Q. Wang, H. Li. Non-contact sensing based geometric quality assessment of buildings and civil structures: a review, *Automation in Construction*, 100:163–179, 2019.

[11] Q. Wang, M.-K. Kim. Applications of 3D point cloud data in the construction industry: A fifteen-year review from 2004 to 2018. *Advanced Engineering Informatics*, 39:306-319, 2019.

[12] Q. Wang, Y. Tan, and Z. Mei, Computational methods of acquisition and processing of 3D point cloud data for construction applications, *Archives of Computational Methods in Engineering*. 27:479–499, 2020.

[13] V. Kasireddy and B. Akinci. Assessing the impact of 3D point neighborhood size selection on unsupervised spall classification with 3D bridge point clouds. *Archives of Computational Methods in Engineering*, 52:101624, 2022.

[14] C. Zhang, J. Shu, H. Zhang, Y. Ning, and Y. Yu. Estimation of load-carrying capacity of cracked RC beams using 3D digital twin model integrated with point clouds and images. *Engineering Structures*, 310:118126, 2024.

[15] J. Shu, C. Zhang, K. Yu, M. Shooshtarian, and P. Liang. IFC-based semantic modeling of damaged RC beams using 3D point clouds. *Structural Concrete*, 24(1):389-401, 2022.

[16] R.B. Rusu. Semantic 3D object maps for everyday manipulation in human living environments. *KI - Künstliche Intelligenz*, 24:345-348, 2010.

[17] F. Li, M.-K. Kim, and D.-E. Lee. Geometrical model based scan planning approach for the classification of rebar diameters. *Automation in Construction*, 130:103848, 2021.